Oxygen Gas Assisted Laser Deposition of Gold Thin Films: Electrooxidation of Glucose

Maxime Gougis[1], Antonio Pereira[2], Dongling Ma[1] and Mohamed Mohamedi[1,*]

[1]Institut National de la Recherche Scientifique (INRS)-Énergie, Matériaux et Télécommunications (EMT), 1650 Boulevard Lionel Boulet, Varennes, Québec, J3X 1S2, Canada.
[2] Institut Lumière Matière - UMR 5306, Université Claude Bernard Lyon 1, 10 rue Ada Byron, 69622, Villeurbanne cedex, France
[*]E-mail: mohamedi@emt.inrs.ca

Gold thin films were deposited onto carbon nanotubes by pulsed laser deposition in presence of moderate O_2 pressures of 10 and 50 mTorr. Structural analysis of the deposited films conducted by means of X-ray diffraction and X-ray photoelectron spectroscopy analyses did not reveal the formation of gold oxide. The electrocatalytic properties of thus synthesized Au thin films were evaluated towards glucose oxidation by cyclic voltammetry, chronoamperometry and square-wave voltammetry. Within the deposited samples, Au thin film fabricated with 50000 laser pulses in presence of 10 mTorr of O_2 displayed a very high electroactive surface area of 16.4 cm^2. At this electrode, the highest sensitivity of 43.6 $\mu A\ cm^{-2}\ mM^{-1}$ up to 20 mM, and a detection limit of at 0.01 mM were obtained by square-wave voltammetry in phosphate buffer saline (PBS, pH 7.2) solution containing concentrations of glucose ranging from 0.01 mM to 100 mM. These results are better than those delivered by Au thin films synthesized under vacuum or inert gas atmosphere.

1. INTRODUCTION

Electrocatalytic glucose oxidation is an important research issue in sensing glucose in blood for medical applications, such as diabetes diagnostics and management [1]. Enzymatic biosensors using glucose oxidase (GOx) are widely employed, but their practical applications are very limited due to low stability, intricate immobilization processes in manufacturing, and oxygen concentrations in the environment [2]. Therefore, enzymeless detection of glucose is being explored as a different approach

to enzymatic sensors but also in the expectation of enhancing the sensitivity and selectivity for blood sugar levels.

There has been a consequent number of reports related to applying Cu, Pt, Pd, Ru, Pb, Bi, Pb, Tl, W and Au metals to glucose non-enzymatic electrochemical sensors. The reader is encouraged to read the excellent and comprehensive reviews of Park et al. [2], Chen et al. [3], and Toghill and Compton [4] for more information. Au is one of the most stable catalyst toward oxidation of glucose and poisoning in neutral and alkaline electrolytes [5], and because of its excellent biological compatibility, gold still retains much attention for the development of different kinds of biosensors. High overpotential of glucose oxidation, poor sensitivity associated to cost are the main obstacles for applying Au as an effective electrochemical glucose non-enzymatic sensor. In order to overcome these problems, numerous approaches were sought towards the use of nanostructured Au in electrodes in recent years [4]. More recent promising approaches include, Au nanoparticle-modified glassy carbon electrodes [6], Au Nanoparticles/Polyaniline Composites [7], nanoporous gold surfaces [8], gold nanostructures on phosphorus doped diamond-like carbon surfaces [9], ordered gold nanowires fabricated by employing anodic aluminum oxide (AAO) templates in combination with direct electrodeposition [10], aligned carbon nanotubes (CNTs) modified carbon fibers coated with gold nanoparticles embedded in a polymer film [11], and anodic fabrication of nanoporous gold films from pure gold in oxalic acid [12].

High activity and low mass loading together with planar deposition techniques could make gold particularly promising for fabrication of miniaturized non-enzymatic glucose electrochemical sensors. The pulsed laser deposition (PLD) technique is a physical method that permits to robustly deposit and control the morphology of ultra-low materials from discrete nanoparticles as small as 2 nm to formation of a continuous ultra-thin layered or multi-layered film with controlled thickness (from 2 to few hundred of nm) by sequential ablation of assorted targets [13]. Another essential characteristic of the PLD is that the stoichiometry of the target is retained in the deposited films which is an advantage over other thin film synthesis methods. All these versatile capabilities make the PLD, a method of choice for the synthesis of model materials for fundamental studies including electrochemical ones and could also make the technique as a production tool for on chip miniature-sized electrochemical sensors in the near future.

Previously, we reported the growth of several Au thin films directly on CNTs substrates using PLD [14]. The morphology of the as-grown Au films was highly influenced by the growth conditions, including the number of laser pulses and the background gas atmosphere in the deposition chamber (vacuum and inert gas such as helium). Among all the synthesized Au nanostructures, it was found that Au film deposited under vacuum displays an electroactive surface area (*ESA*) of 6.55 cm^2 and a roughness factor of 13.2. In cyclic voltammetric (CV) and square-wave voltammetric (SWV) studies carried out in phosphate buffer saline (PBS, pH 7.2) containing various concentrations of glucose, this electrode offered a sensitivity of 25 μA cm^{-2} mM^{-1} and an extended calibration range from 0.1 mM to 50 mM of glucose.

In this study, an investigation of the electrocatalytic properties of gold thin films deposited by PLD deposited onto CNTs substrate in presence of an oxygen atmosphere is conducted. Thus synthesized Au films are characterized by field emission scanning electron microscopy (FESEM), X-

ray diffraction (XRD), X-Ray photoelectron spectroscopy (XPS) and transmission electron microscopy (TEM). The main focus of this work is to evaluate the electrochemical properties of these Au thin films towards the glucose electrooxidation and sensitivity. This is done with CV, chronoamperometry and SWV in a pH 7.2 PBS containing glucose over a large range of concentrations from 0.01 mM to 100 mM.

2. EXPERIMENTAL

2.1. Materials synthesis

PLD-deposited nickel film was used as the catalyst for the growth of CNTs onto carbon paper (CP, Toray). The CNTs were grown by CVD at 700°C using acetylene (carbon source), hydrogen and argon (gas carrier) with flow rates of 20, 140 and 100 sccm, respectively. Full experimental details regarding the synthesis of the CNTs can be found elsewhere [15].

Gold thin film was deposited on CNTs by PLD at room temperature by means of a pulsed KrF excimer laser (λ = 248 nm, pulse width = 17 ns, and repetition rate = 50 Hz) and by using a pure polycrystalline Au target (99.99%, Kurt J. Lesker Co.). Prior to deposition, the PLD chamber was evacuated with a turbo pump (2×10^{-5} Torr). The fluence was fixed to 4 J cm^{-2} and the target-to-substrate distance was set to 50 mm. The Au catalyst films were deposited under two pressures of oxygen, 10 mTorr and 50 mTorr. Two deposits with number of pulses of 10000 (10 kp) and 50000 (50 kp) were made for each pressure value. During deposition, the Au target was continuously rotated and translated in order to obtain a uniform ablation over the entire target surface. The duration to deposit Au in presence of O_2 with 10 kp lasts about 200 seconds, whereas the one with 50 kp takes around 1000 seconds. The four Au catalysts considered in this work are denoted $(Au10kp)_{10mT}$, $(Au10kp)_{50mT}$, $(Au50kp)_{10mT}$ and $(Au50kp)_{50mT}$, where the subscript T stands for Torr. A detailed description of the PLD setup has been given elsewhere [16].

2.2. Characterization

The morphologies of the CNT/Au structures were examined by means of FESEM (JEOL-JSM-7600) and TEM (JEOL-JEM-2100F operating at 200 kV). The surface composition was studied by XPS via a VG Escalab 220i-XL equipped with an Al Kα source (1486.6 eV). The anode was operated at 10 kV and 20 mA. The pass energy of the analyzer was fixed at 20 eV. All samples were analyzed with a spot size of 250×1000 μm located approximately in the center of the samples. A survey spectrum ranging from 0 to 1300 eV was first acquired and then higher resolution multiplex scan spectra of Au 4f were obtained. The crystalline structure of all samples was determined by XRD using a Bruker D8 Advance diffractometer equipped with a Cu Kα source. The diffractometer was operated at 40 kV and 40 mA. All diffractograms were acquired in the Grazing Incidence Diffraction (GID) scan mode with an incident angle of 2°, 2θ angular step size of 0.05° and acquisition time of 5 seconds per step.

2.3. Electrochemical measurements

Prior to the electrochemical measurements, the surface of the working electrode was cleaned electrochemically by potential cycling in 0.5 M H_2SO_4. The electrochemical properties of the Au electrodes were investigated using CV and SWV in a deaerated PBS solution (pH=7.2, Sigma-Aldrich) with glucose (D-(+)-Glucose, ACS reagent grade, Sigma-Aldrich). All the electrochemical measurements were carried out at room temperature using a three compartment electrochemical cell with an Ag/AgCl, 3 M NaCl reference electrode and a platinum coil as a counter electrode. Measurements and data acquisition were conducted with an Autolab potentiostat/galvanostat from Eco Chemie.

3. RESULTS AND DISCUSSIONS

3.1. Structural characterization

Figure 1 shows typical FESEM images of the various Au films grown in the presence of oxygen onto CNTs. No major differences in the surface topography could be noticed between the various deposits. The CNTs are densely covered by Au film of closed structure. A CNT covered with Au film looks as quasi-one-dimensional nanostructure. The high magnification images suggest that the average width of the (CNT+Au) tube is about, 26 nm, 26 nm, 116 nm and 85.3 nm for $(Au10kp)_{10mT}$, $(Au10kp)_{50mT}$, $(Au50kp)_{10mT}$ and $(Au50kp)_{50mT}$, respectively. The mean outer diameter of our CNTs are around 12 nm [15], which yields to an average Au film thickness of 14 nm, 14 nm, 104 nm and 73 nm obtained for $(Au10kp)_{10mT}$, $(Au10kp)_{50mT}$, $(Au50kp)_{10mT}$ and $(Au50kp)_{50mT}$, respectively. At first glance with FESEM, the morphology of Au films deposited in presence of oxygen is similar to Au film deposited under vacuum but very different from Au deposits in the presence of He gas, where it was observed that Au films are porous and made of particles that tend to gather into highly compacted large grains [14].

In Figure 2, the TEM and HR-TEM images show that the morphology of Au deposits is a mixture of well-separated nanoparticles attached to the outer walls of the CNT and a continuous Au film along the basal-plane like surface of the CNTs. The particle size distribution revealed an average size of 5.1 nm, 5.3 nm, 5.8 nm and 5.1 nm is observed for $(Au10kp)_{10mT}$, $(Au10kp)_{50mT}$, $(Au50kp)_{10mT}$ and $(Au50kp)_{50mT}$, respectively.

The typical XRD histograms of Au films grown in the presence of an O_2 atmosphere at various pressures are shown in Fig. 3A. The XRD profile of pure Au deposited under vacuum is shown a as benchmark. The histograms of Au films made under O_2 atmosphere display similar patterns to those of pure Au, that is to say the diffraction peaks at $2\theta = 38.2^o$, 44.4^o, 64.6^o, 77.5^o, and 81.8 corresponding respectively to {111}, {200}, {220}, {311}, and {222} reflections, respectively (JCPDF 89-3697). This indicates that metallic gold is present in all films deposited under oxygen. It seems thus that no gold oxide has been formed.The XRD histogram of Au deposited under vacuum displays all the characteristic diffraction peaks of polycrystalline (powdered) Au, whereas the XRD histograms of Au deposited in presence of O_2 shows the characteristics of a mixture of highly oriented in the (111)

direction and polycrystalline Au [17]. By using the Debye-Scherrer equation and the most intense (111) diffraction peak, the average crystallite size was estimated to range between 12 and 20 nm, whereas the lattice parameter was determined to be within 4.075 and 4.077 Å. It has be noted that, Au films deposited under vacuum or He gas atmosphere displayed an average crystallite size within 20 and 35 nm [14], which is larger than those observed here.
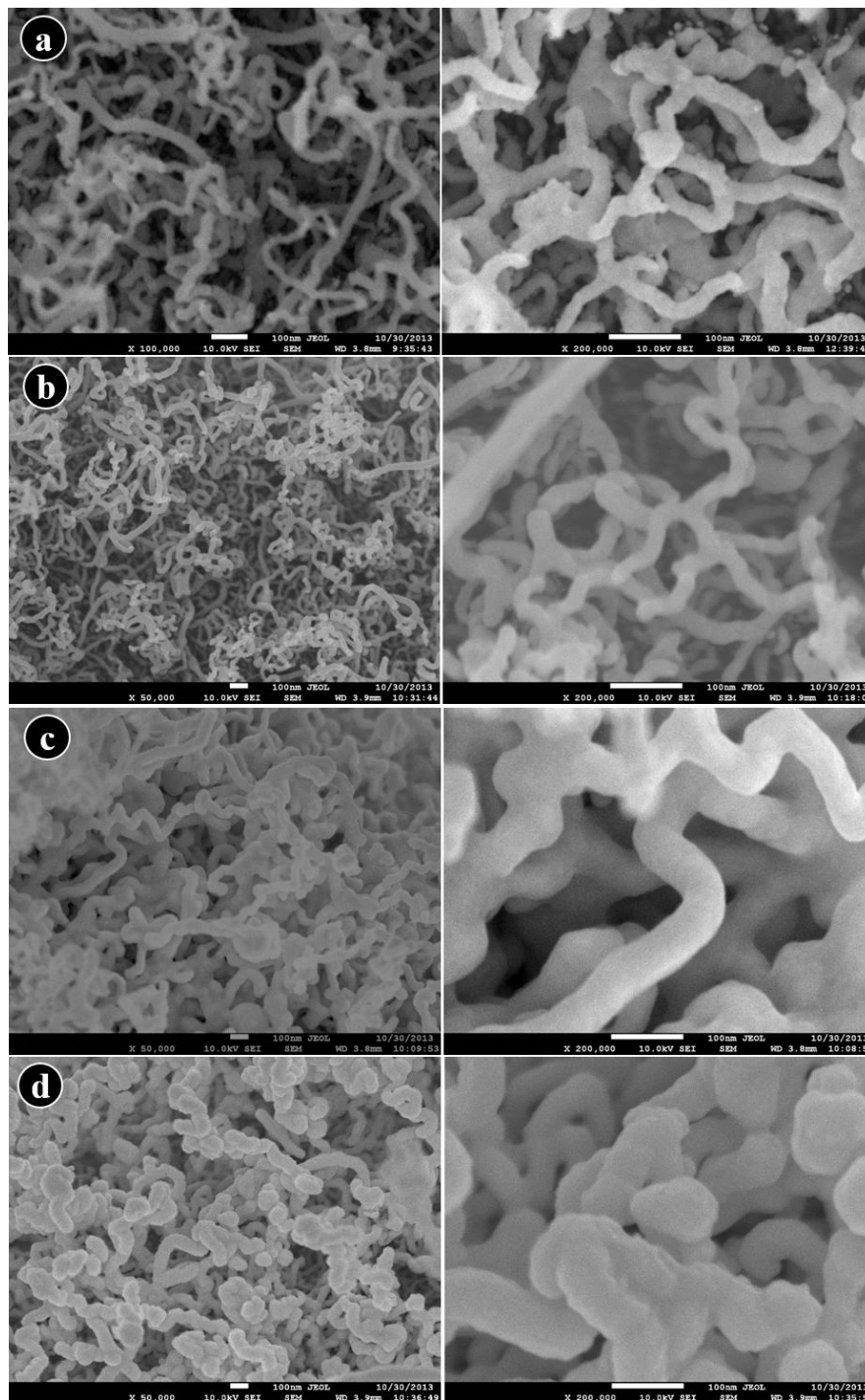

Figure 1. FESEM images of gold PLD-deposited onto carbon nanotubes in presence of oxygen: (a) $(Au10kp)_{10mT}$, (b) $(Au10kp)_{50mT}$, (c) $(Au50kp)_{10mT}$ and (d) $(Au50kp)_{50mT}$.
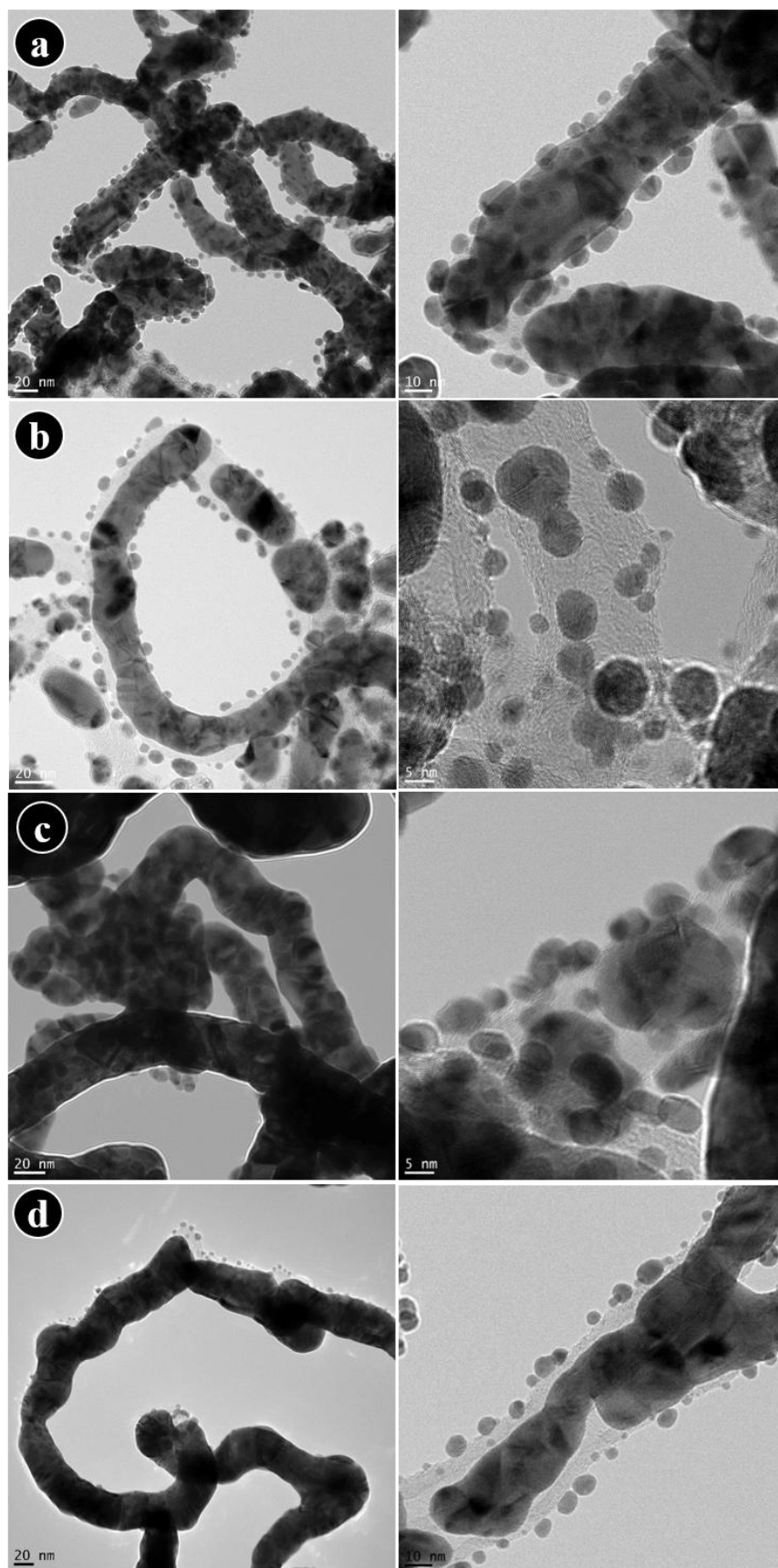
Figure 2. TEM and HR-TEM analyses of gold PLD-deposited onto carbon nanotubes in presence of oxygen: (a) $(Au10kp)_{10mT}$, (b) $(Au10kp)_{50mT}$, (c) $(Au50kp)_{10mT}$ and (d) $(Au50kp)_{50mT}$.
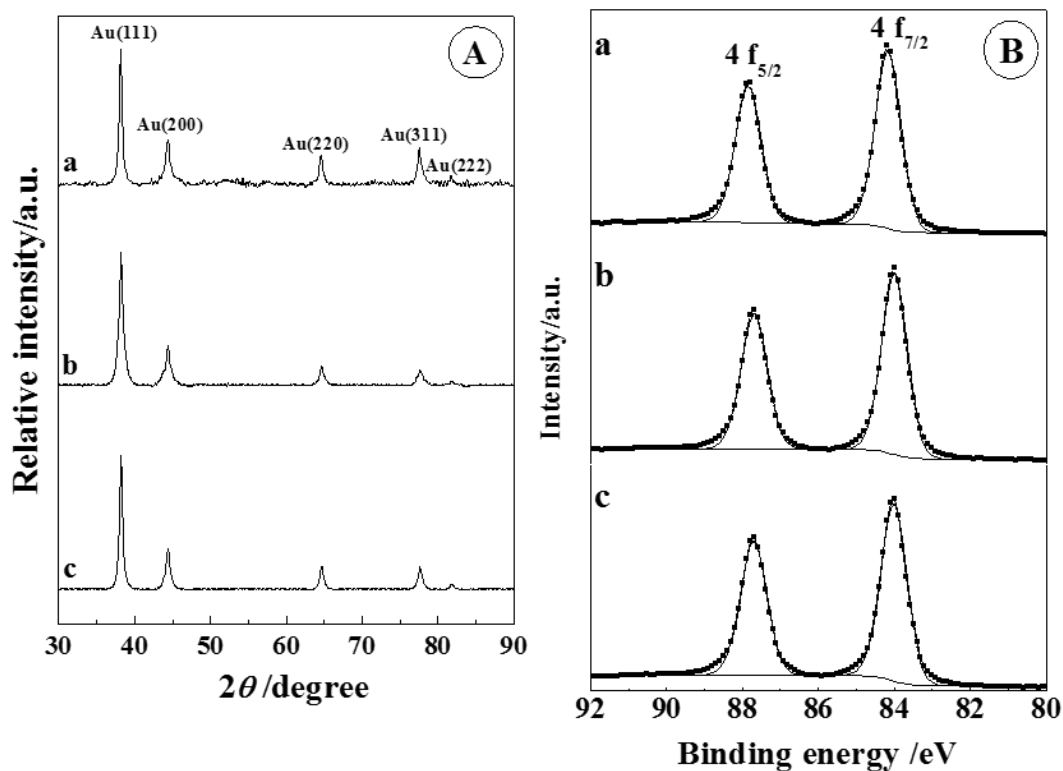
Figure 3. (A) XRD patterns and (B) High-resolution XPS spectra in the Au 4f region. (a) Under vacuum $(Au50kp)_{UV}$, (b) $(Au50kp)_{10mT}$, (c) $(Au50kp)_{50mT}$.

High-resolution XPS spectra in the Au 4f region of Au films grown in presence of O_2 are shown in Fig. 3B. For comparison, the XPS spectrum of an Au film grown under vacuum is also reported in Fig. 3B. The spectra of Au film grown in the presence of O_2 display two $4f_{7/2}$ and $4f_{5/2}$ core levels whose maximum intensities are located at binding energy of 84.0 ± 0.1 and 87.7 ± 0.1 eV. There is a 3.7 ± 0.1 eV energy difference between the $4f_{7/2}$ and $4f_{5/2}$ components, which is consistent with gold being in the metallic state [18]. No other chemical states of Au were identified and satisfactory fitting of each core level peak was obtained using only one component with an asymmetric profile. The full width at half maximum (FWHM) of the gold component is of 0.8 eV for all the samples, which confirms the absence of gold oxide phase [19]. The absence of gold oxide revealed by XPS is thus in line with XRD observations.

3.2. Electrochemical characterization

ESA was determined by CV at 50 mV s^{-1} potential scan rate in a 0.5 M H_2SO_4 solution in the potential range of 0 V to 1.6 V vs Ag/AgCl. The corresponding CV profiles are shown in Fig. 4. The anodic currents starting at 1.10 V are due to the formation of Au oxides [20]. Subsequently, in the negative potential scan, they are reduced, as indicated by the appearance of a peak at about 0.95 V. By integrating the charge consumed for reducing the Au oxides formed in the positive

scan, the *ESA*s of the electrodes were calculated by assuming that the reduction of a monolayer of Au oxides requires 400 μC cm^{-2} [21] and the results are listed in Table 1. First, it can be seen that Au films grown under oxygen displayed *ESA* remarkably greater than the Au film grown under vacuum. More striking is the electroactivity exhibited by the (Au50kp)$_{10mT}$ with an *ESA* of 16.4 cm^2, which is much superior than commercial flat Au electrode (*ESA*=0.155 cm^{-2}) [22], or than that of pure Au wire electrode (*ESA*=0.138 cm^2) [23], and PLD-Au film grown in presence of helium atmosphere (*ESA*=4.49 cm^2) [14]. For comparison, an *ESA* of 4 cm^2 was obtained with a flower-like submicrometer gold particles [24], 2.5 cm^2 with CNT/Au-NPs-glassy carbon spheres [25], 2.23 cm^2 with 3D ordered microporous Au film [26], 1.08 cm^2 with electrodeposited Au NPs onto InO$_2$ film coated glass [27], 2 cm^2 with cylindrical and macroporous Au microelectrodes [28], 5 cm^2 with Au deposited onto carbon spheres chains [23], and 1.81 cm^2 obtained with Au nanocoral electrode [22] to name a few. The roughness factor (*RF*) estimated by dividing the *ESA* by the geometric area of the electrode is reported in Table 1. Here too, Au films grown in the presence of O$_2$ showed an RF higher than Au$_{UV}$ film and Au films grown in presence of a helium atmosphere [14]. Within the Au films made under O$_2$, the (Au50kp)$_{10mT}$ electrode outperforms the other electrodes with an RF of 34.2 (Table 1).

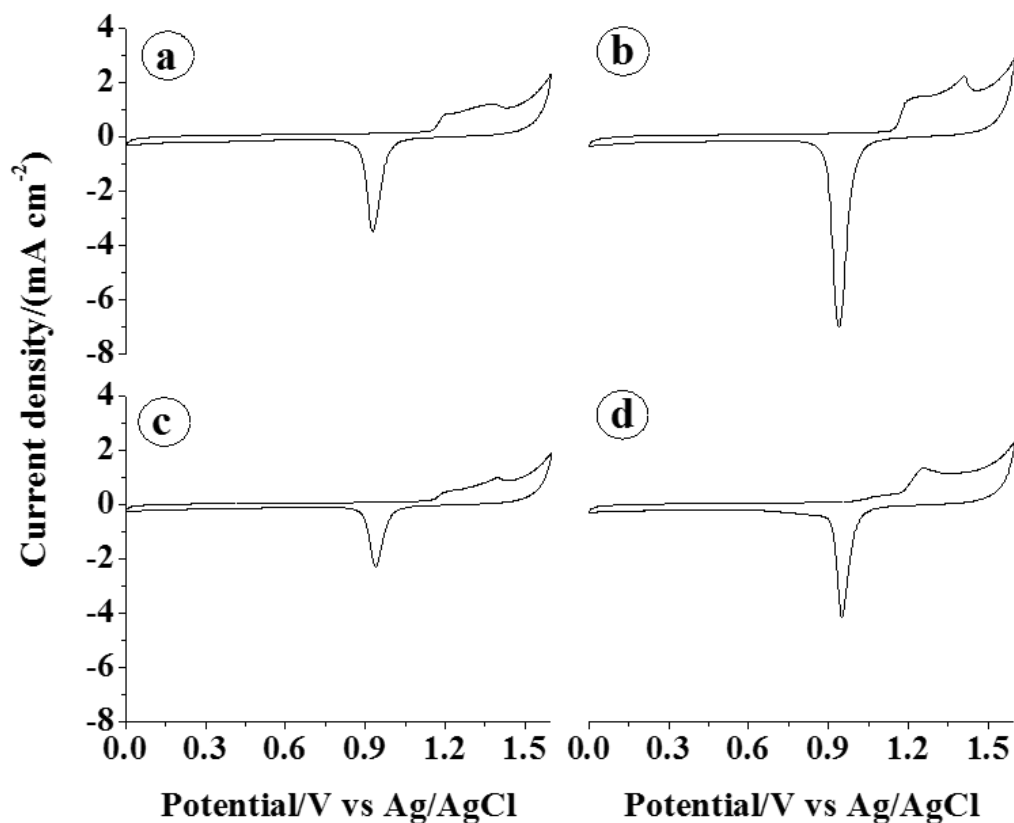**Figure 4.** CV recorded with 50 mV s^{-1} potential scan rate in a de-aerated solution of 0.5 M H$_2$SO$_4$ at the various Au electrodes. (a) (Au10kp)$_{10mT}$, (b) (Au50kp)$_{10mT}$, (c) (Au10kp)$_{50mT}$ and (d) (Au50kp)$_{50mT}$.

Table 1. *ESA* and *RF* parameters estimated from CVs of Fig. 4.

Electrode	*ESA* (cm^2)	*RF*
(Au50kp)$_{UV}$	3.88	8.13
(Au10kp)$_{10mT}$	9.57	17.9
(Au10kp)$_{50mT}$	5.58	10.5
(Au50kp)$_{10mT}$	16.4	34.2
(Au50kp)$_{50mT}$	9.63	16.7

Subsequently, we focused on investigating the electrocatalytic activity of the (Au50kp)$_{10mT}$ electrode toward the oxidation of glucose. Figure 5a shows the CV of the oxidation of glucose at the (Au50kp)$_{10mT}$ electrode in a pH 7.2 PBS solution containing 7 mM of glucose at 2 mV s^{-1} (quasi-steady state). The electrode displayed the typical response of glucose oxidation at Au electrode [22]. The CV in the forward scan process displayed two anodic current peaks P1 and P2 located at 0.22 and 0.34 V vs. Ag/AgCl, respectively. The electrocatalytic behaviour of gold is extremely complex, and despite numerous investigations, the exact mechanism for glucose oxidation at gold remains unestablished. The reader is directed to the review of Toghill and Compton for further information regarding the different mechanisms proposed for glucose oxidation at gold electrode [4]. One of the mechanism generally accepted in the literature claims that the catalytic component of gold electrode is believed to be hydrous gold oxide, AuOH, which is formed by the chemisorption of hydroxide anions to the gold surface [4, 29-30]. Accordingly, the first peak P1 observed in the CV of Fig. 5a should be due to the electrosorption of glucose to form adsorbed intermediate, releasing one proton per glucose molecule. Alongside with the electrosorption of glucose, the adsorbed intermediates accumulate and inhibit the active sites of the gold surface resulting in a decrease of the current. With the potential moving forward, AuOH species begin to form and catalyze the oxidation of the poisoning intermediates, releasing gold active sites for the direct oxidation of glucose and the second current peak P2 at 0.34 V for this direct oxidation appears. The decrease in current after the second peak is due to the formation of gold oxide, which competes for adsorption sites with glucose, inhibiting the further electrochemical oxidation of glucose as well. In the backward potential scan process, the gold oxide species are reduced leading to an anodic peak P3 at 0.37 V.

Afterwards, slow scan cyclic voltammetry with 2 mV s^{-1} was conducted in a PBS solution containing various concentrations of glucose (0.01 mM to 100 mM) at the (Au50kp)10mT electrode in order to evaluate its detection capabilities of glucose. The results of Fig. 5b show that both current peaks P1 and P2 increased as the concentration of glucose increased. Next, for each concentration of glucose the maximum current (peak current) related to both peaks were measured and are reported as function of glucose concentration and the corresponding calibration curves are reported in Fig. 5c and Fig. 5d. The variation of the current peak P1 with glucose concentration exhibit a linear range (R^2=0.9930) from 0 to 10 mM with a sensitivity of 18.2 μA cm^{-2} mM^{-1} and a low detection limit of 0.01 mM. It should be noted that the first peak is barely seen at concentration of glucose higher than 10 mM.
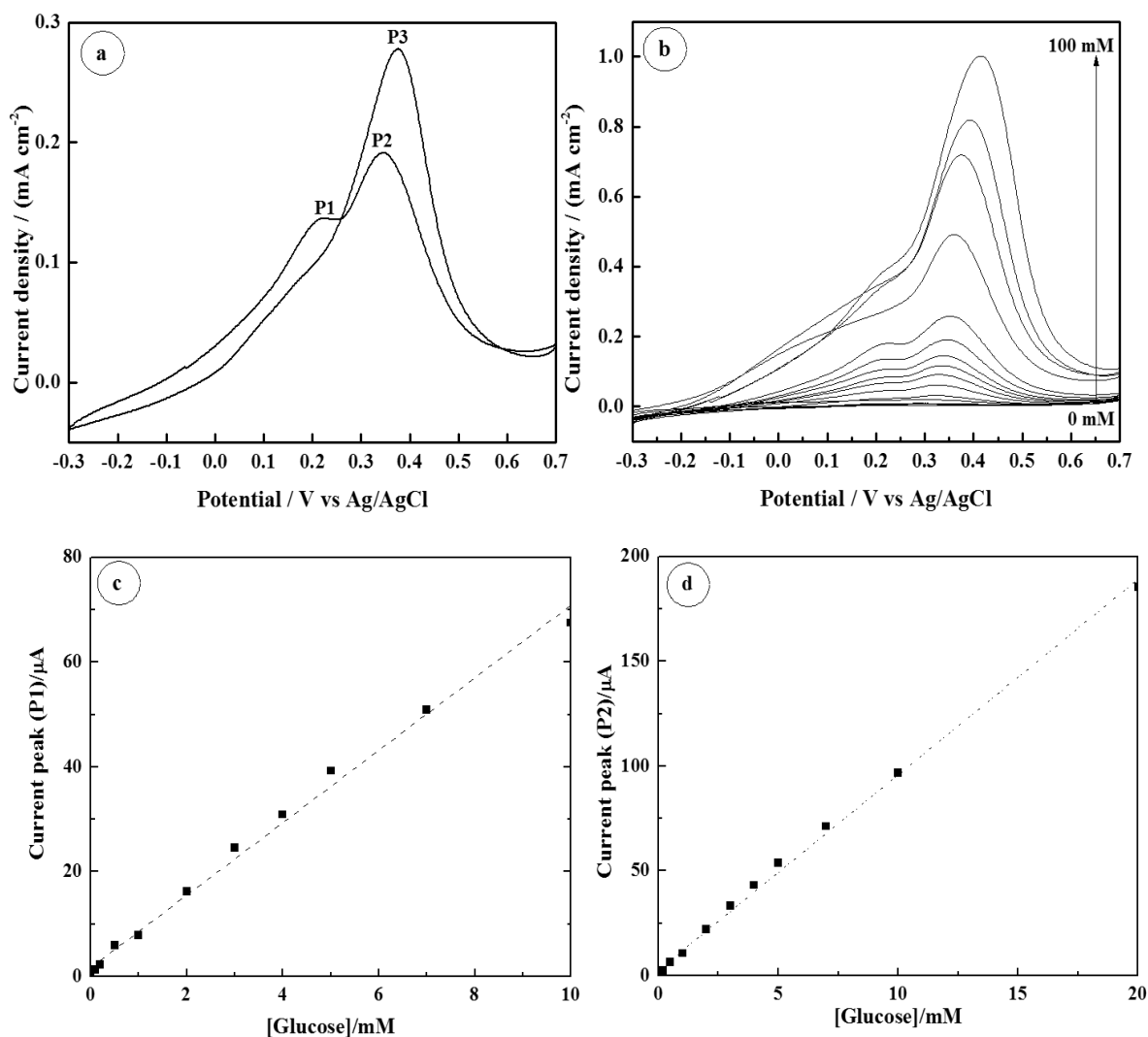
Figure 5. Voltammetry measurements recorded at the $(Au50kp)_{10mT}$ electrode in argon-saturated 0.01 M PBS solution at pH 7.2 containing glucose. (a) CV with 2 mV s^{-1} in PBS+ 7 mM of glucose. (b) CVs with 2 mV s^{-1} in PBS containing concentrations of glucose varying from 0.01 mM to 100 mM. (c) The linearity domain of current peak P1. (d) The linearity domain of current peak P2.

On the other hand, the current peak P2 displays a linear range (R^2=0.9970) over 0 to 20 mM range far beyond the physiological level (3-8 mM), a sensitivity of 24.6 $\mu A\ cm^{-2}\ mM^{-1}$, and a low detection limit of 0.01 mM.

Chronoamperometric measurements with successive increments of glucose concentration 0.01 M PBS solution at pH 7.2 were conducted at applied potentials of 0.25 V (Fig. 6a) and 0.3 V vs Ag/AgCl (Fig. 6c). A sensitivity of 33 and 35.6 $\mu A\ cm^{-2}\ mM^{-1}$ within a range from 0 to 10 mM were obtained at 0.25 V (Fig. 6b) and 0.3 V vs Ag/AgCl (Fig. 6d), respectively.

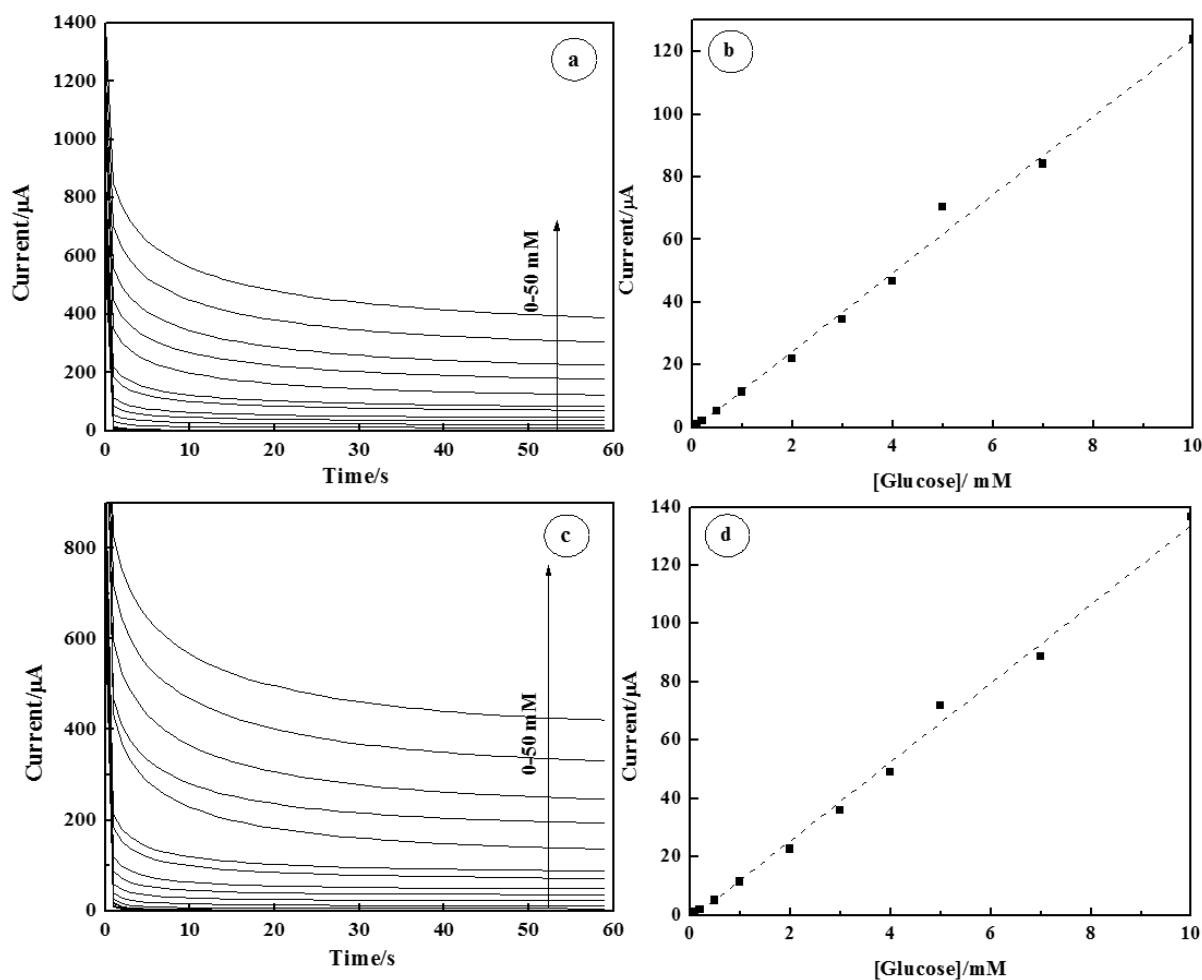**Figure 6.** Chronoamperometry measurements recorded at the $(Au50kp)_{10mT}$ electrode in argon-saturated 0.01 M PBS solution at pH 7.2 containing concentrations of glucose varying from 0 to 50 mM. (a) Chronoamperograms recorded at an applied potential of 0.25 V vs Ag/AgCl and (b) linearity domain. (c) Chronoamperograms recorded at an applied potential of 0.30 V vs Ag/AgCl and (d) linearity domain.

The SWV technique was also considered to seek out potential sensitivity enhancements since it is a pulse method that can differentiates between the charging currents and the faradaic process principally at very low concentrations of the solute [31]. Figure 7a shows SWVs recorded with an amplitude of 20 mV, a step potential of 1 mV and a frequency of 20 Hz at the $(Au50kp)_{10mT}$ electrode in argon-saturated 0.01 M PBS solution at pH 7.2 containing various concentrations of glucose ranging from 0.01 mM to 100 mM. Well-defined and well-separated SWV peaks were obtained as compared to CVs of Fig. 5b. Here too, the peak P1 is no longer seen at glucose concentrations greater than 10 mM.
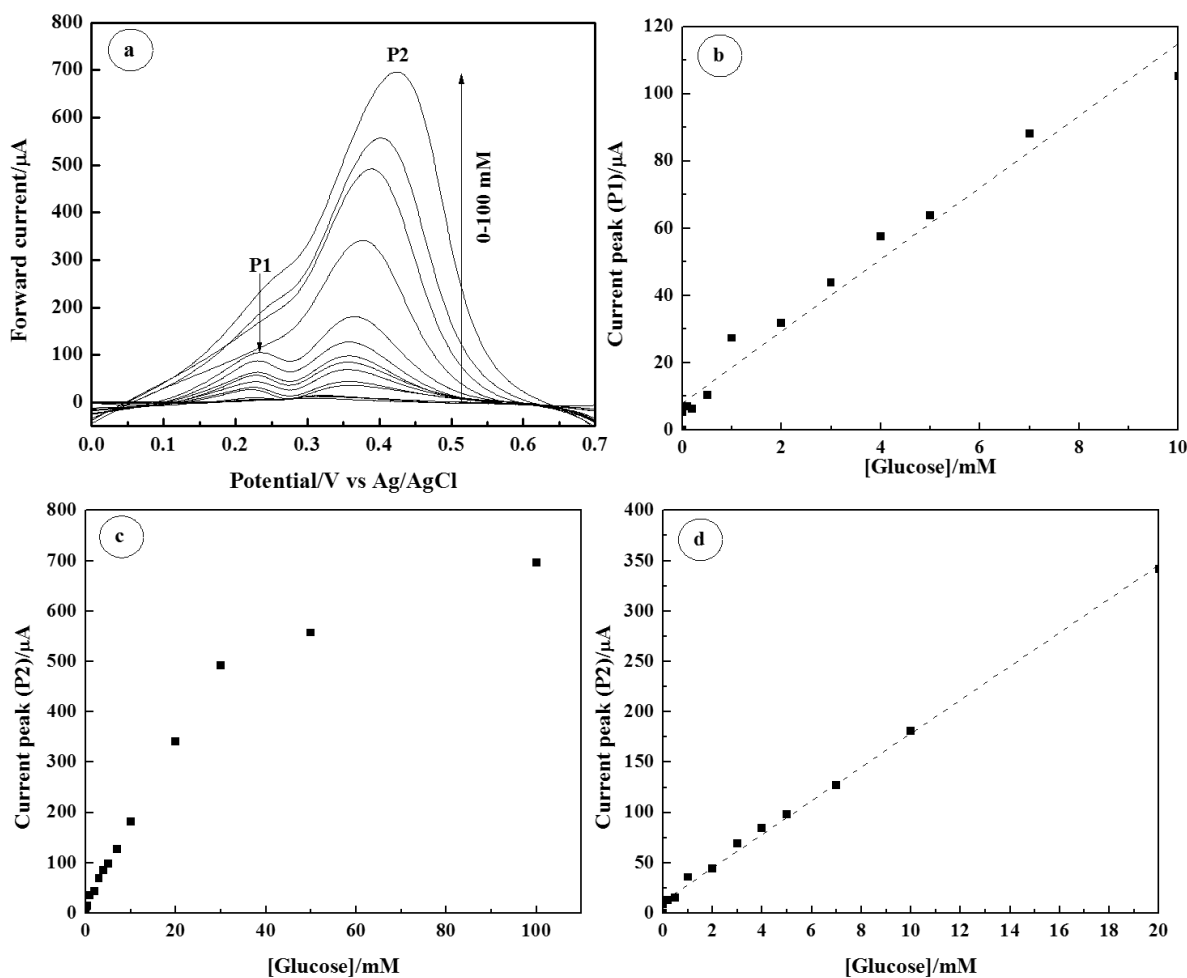
Figure 7. (a) Square-wave voltammograms recorded with an amplitude of 20 mV, a step potential of 1 mV and a frequency of 20 Hz at the $(Au50kp)_{10mT}$ electrode in PBS containing concentrations of glucose varying from 0.01 mM to 100 mM. (b) The linearity domain of current peak P1. (c) The dependence of the current peak P2 over the whole concentration range. (d) The linearity domain of current peak P2.

The corresponding calibration curve related to peak P1 is shown in Fig. 7b. The linear range for glucose concentration is 0.01-10 mM with a fair linear dependence (R^2=0.9700), a detection sensitivity of 28.2 $\mu A\ cm^{-2}\ mM^{-1}$. On the other hand, the second current peak P2 showed a linear dependence up to 20 mM (Fig. 7c) with a regression factor of 0.9977 (Fig. 7d). The sensitivity was found to be 43.6 $\mu A\ cm^{-2}\ mM^{-1}$, and a low detection limit of 0.01 mM. The sensitivity obtained with SWV technique is much better than the one determined by chronoamperometry and CV, and the acquisition time is also much shorter with SWV.

Indeed, the PLD deposition in an atmosphere of oxygen results in the dissociation of O_2 molecules and the production of atomic oxygen which reacts with the gold to form an oxide [32]. However, such mechanism was observed only for oxygen pressures higher than 13.3 Pa (~100 mTorr) [19]. The O_2 pressures used in this work are lower and this why gold oxide was not formed in our deposits. In addition, it would not be interesting for us to deposit the gold oxide given that it

is highly resistive and insulating. The relationship between the deposition parameters (background gas, gas pressure) and the structure of the gold thin films is not a simple one. It can only be obtained by a thorough study of the plasma expansion dynamics in the PLD deposition conditions leading to the preparation of the films. The analysis of these changes is too specialized and is beyond the scope of this study.

A proven fact of this work is that synthesizing Au thin films in the presence of moderate pressures of oxygen greatly improves the electrochemical properties towards oxidation and detection of glucose as compared with Au thin films fabricated under vacuum or inert gas atmosphere. The good performance of the (Au50kp)$_{10mT}$ electrode can presumably be attributed to its surface morphology, which offers an *ESA* greater than Au thin films synthesized under vacuum or inert atmosphere such as helium [14].

4. CONCLUSIONS

In this study, the pulsed laser deposition method has been employed to synthesize gold nanostructures in presence of oxygen gas on carbon nanotubes electrodes and evaluate their electroanalytical properties toward glucose oxidation. Under the conditions of O_2 pressures used, XRD and XPS analyses did not reveal the formation of gold oxide. The CNTs were coated with well-separated Au nanoparticles on their outer walls and densely covered with a continuous Au film along their basal-plane like surface as revealed by TEM images.

Among the electrodes fabricated, the (Au50kp)$_{10mT}$ electrode synthesized with 50000 laser pulses (~73 nm thickness) under 10 mT of O_2 pressure showed a very high electroactive surface area of 16.4 cm^2. By means of CV, chronoamperometry and SWV electroanalytical methods, the electrocatalytic and sensing properties towards glucose of the (Au50kp)$_{10mT}$ electrode were investigated in PBS solution containing various concentrations of glucose ranging from 0.01 mM to 100 mM. The highest sensitivity for glucose oxidation is estimated to be 43.6 μA cm^{-2} mM^{-1} up to 20 mM based on SWV results, whereas the detection limit is observed at 0.01 mM, which is a significant enhancement compared to Au films deposited under vacuum or inert gas atmosphere. Considering that the normal physiological level of glucose (3-8 mM), this electrode is potentially suitable for enzymeless glucose sensor.

References

1. A. Heller, B. Feldman, *Chem. Rev.*, 108 (2008) 2482.
2. S. Park, H. Boo, T. D. Chung, Anal. *Chim. Acta*, 556 (2006) 46.
3. C. Chen, Q. Xie, D. Yang, H. Xiao, Y. Fu, Y. Tan, and S. Yao, *RSC Adv.*, 3 (2013) 4473.
4. K. E. Toghill, R. G. Compton, *Int. J. Electrochem. Sci.*, 5 (2010) 1246.
5. R. R. Adzic, M. W. Hsiao, E. B. Yeager, *J. Electroanal. Chem.*, 260 (1989) 475.

6.   Sami Ben Aoun, *Int. J. Electrochem. Sci.*, 8 (2013) 10454.

7.   M. Guerra-Balcázar, R.Ortega, F. Castaneda, L.G. Arriaga, J. Ledesma-Garcia, *Int. J. Electrochem. Sci.*, 6 (2011) 4667.

8.   a) H. Jeong, J. Kim, *Electrochim. Acta*, 80 (2012) 383; b) B. Seo, and J. Kim, *Electroanalysis*, 22 (2010) 939.

9.   A. Liu, Q. Ren, T. Xu, M. Yuan, W. Tang, *Sens. Actuator B-Chem.*, 162 (2012) 135.

10. Q. Wang, F. Min, J. Zhu, *Mat. Lett*., 91 (2013) 9.

11. B. Sebez, L. Su, B. Ogorevc, Y. Tong, X. Zhang, *Electrochem. Commun.*, 25 (2012) 94.

12. Shili Xu, Yuan Yao, Pengshu Wang, Yingchang Yang, Yue Xia, Jun Liu, Zelin Li, Wei Huang, *Int. J. Electrochem. Sci.*, 8 (2013) 1863.

13. D. B. Chrisey and G. K. Hubler, *Pulsed Laser Deposition of Thin Films*, Wiley, New York (1994).

14. M. Gougis, A. Tabet-Aoul, D. Ma and M. Mohamedi, *Sens. Actuator B-Chem.*, B193 (2014) 363.

15. A. Tabet-Aoul, F. Saidani, D. Rochefort and M. Mohamedi, *Int. J. Electrochem. Sci.*, 6 (2011) 6385; A. Tabet-Aoul, M. Mohamedi, *J. Mater. Chem.*, 22 (2012) 2491.

16. E. Irissou, F. Vidal, T. W. Johnston, M. Chaker, D. Guay, A. N. Ryabinin, *J. Appl. Phys*., 99 (2006) 034904.

17. E. Irissou, B. Le Drogoff, M. Chaker, and D. Guay, *Appl. Phys. Lett*., 80 (2002) 1716.

18. M. P. Seah, G. C. Smith, M. T. Anthony, *Surf. Interface Anal.*, 15 (1990) 293.

19. E. Irissou, M.-C. Denis, M. Chaker, D. Guay, *Thin Solid Films*, 47 (2005) 249.

20. S. Trasatti, O. A. Petrii, *Pure Appl. Chem*., 63 (1991) 711.

21. H. A. Kozlowska, B. E. Conway, A. Hamelin, L. Stoicoviciu, *J. Electroanal. Chem.*, 228 (1987) 429.

22. T. M. Cheng, T. K. Huang, H. K. Lin, S. P. Tung, Y. L. Chen, C. Y. Lee, H. T. Chiu, *ACS Appl. Mater. Interfaces*, 2 (2010) 2773.

23. A. Tabet-Aoul, M. Mohamedi, *Electrochem. Commun.*, 13 (2011) 534.

24. C. Shan, D. Han, J. Song, A. Ivaska, L. J. Niu, *J. Mater. Res.*, 25 (2010) 1755.

25. X. Dai, G. G. Wildgoose, C. Salter, A. Crossley, R. G. Compton, *Anal. Chem.*, 78 (2006) 6102.

26. H. Wu, F. Bai, Z. Sun, R. E. Haddad, D. M. Boye, Z. Wang, J. Y. Huang, H. Fan*, J. Am. Chem. Soc.*, 132 (2010) 12826.

27. X. Dai, R. G. Compton, *Anal. Sci.*, 22 (2006) 567.

28. S. Reculusa, M. Heim, F. Gao, N. Mano, S. Ravaine, A. Kuhn, *Adv. Funct. Mater.*, 21 (2011) 691.

29. Y. Li, Y. Y. Song, C. Yang, X. H. Xia, *Electrochem. Commun.*, 9 (2007) 981.

30. H. Zhang, J.-J. Xu, and H.-Y. Chen, *J. Phys. Chem. C*, 112 (2008) 13886.

31. M. Lovric, *Guide to experiments and applications*, (Eds.: F. Scholz), Electroanalytical Methods, Springer, Berlin (2005) pp. 111-136.

32. A. Camposeo, F. Cervelli, F. Fuso, M. Allegrini and E. Arimondo, *Appl. Phys. Lett.*, 78 (2001) 2402.